

Statistics of Velocity Gradients in Two-Dimensional Navier-Stokes and Ocean Turbulence

Norbert Schorghofer

*Department of Earth, Atmospheric, and Planetary Sciences,
Massachusetts Institute of Technology, Cambridge, MA 02139*

Sarah T. Gille

*Scripps Institution of Oceanography and Department of Mechanical and Aerospace Engineering,
University of California San Diego, La Jolla, CA 92093-0230*

(Dated: November 11, 2018)

Probability density functions and conditional averages of velocity gradients derived from upper ocean observations are compared with results from forced simulations of the two-dimensional Navier-Stokes equations. Ocean data are derived from TOPEX satellite altimeter measurements. The simulations use rapid forcing on large scales, characteristic of surface winds. The probability distributions of transverse velocity derivatives from the ocean observations agree with the forced simulations, though they differ from unforced simulations reported elsewhere. The distribution and cross-correlation of velocity derivatives provide clear evidence that large coherent eddies play only a minor role in generating the observed statistics.

PACS numbers: 47.27.Eq, 92.10.Fj, 92.10.Lq

I. INTRODUCTION

Statistical properties of turbulent flows, such as probability density functions (pdfs), are important for characterizing turbulence. For instance, velocity gradients are directly related to velocity correlations, relative dispersion, and energy dissipation in the fluid [1]. This study evaluates statistics of turbulence, as observed in recent satellite measurements of the upper ocean. Statistics of observed phenomena are compared with corresponding statistics for the forced two-dimensional Navier-Stokes equations. Our results show that, in comparison with unforced decaying turbulence, simple forced two-dimensional Navier-Stokes equations provide better agreement with ocean observations.

For this analysis, ocean velocities are derived from altimeter data collected by the TOPEX/POSEIDON satellite, which performs repeated measurements of the height η of the ocean surface. We use only observations from the TOPEX altimeter, which has lower noise levels than the POSEIDON instrument. The geostrophic relation, $v_x = (g/f)\partial\eta/\partial y$, yields the velocity component perpendicular to the satellite ground track. Surface geostrophic velocities are characteristic of sub-surface flow in the ocean [2]. This geostrophic flow is typically well-represented by two-dimensional shallow-water equations and resembles two-dimensional turbulence [3, 4]. The derivative along the satellite track, $\partial_y v_x$, yields the transverse velocity gradient. We compute velocities v from consecutive high-frequency altimeter measurements [5, 6, 7, 8], and then determine velocity gradients by computing along track differences over a distance of 12 km. For comparison, the first baroclinic Rossby radius ranges between 10 km and 80 km between 60° and 10° latitude [9, 10], so transverse gradients over 12 km distance are expected to be representative of mesoscale geostrophic motions. The cross-

track, or longitudinal, derivative cannot be determined. Higher order derivatives are increasingly noisy.

Earlier results have shown that velocities typically have Gaussian distributions within small regions of the ocean. When satellite data from the global ocean were combined, the resulting pdfs were non-Gaussian, due to regional variations in velocity variance [7, 8]. When velocities were normalized by their local variances, the pdfs were Gaussian [8], at least for well-sampled velocities within three standard deviations of the mean. Similar results were obtained for subsurface floats deployed in the North Atlantic Ocean, although analysis for velocities more than three standard deviations from the mean indicated non-Gaussian tails [11]. The Lagrangian statistics of floats are however not directly comparable to the results from the TOPEX altimeter, which captures the Eulerian statistics. In this study, we specifically normalize velocities and velocity gradients by their local variances before computing pdfs and other statistics.

We compare observed oceanic pdfs with simulations of two-dimensional quasi-geostrophic flow. The equations of motion are

$$\left(\frac{\partial}{\partial t} + \frac{\partial\psi}{\partial y}\frac{\partial}{\partial x} - \frac{\partial\psi}{\partial x}\frac{\partial}{\partial y}\right)q = D\nabla^2 q + F, \quad (1)$$

where the potential vorticity $q = -\nabla^2\psi + \psi/R^2$. The second term in the potential vorticity is neglected both in the quasi-geostrophic limit of the shallow water equations and when the Rossby radius R is large in the homogeneous quasi-geostrophic equations. In either case, eq. (1) is equivalent to two-dimensional Navier-Stokes flow. In this study, we perform simulations of the Navier-Stokes equations. Rapidly varying (white-in-time) forcing F is applied on large scales, through random stirring of the low vorticity modes. This forcing resembles wind forcing of the ocean, which varies rapidly in time but slowly in

space [12, 13]. We consider an isotropic, homogeneous, and statistically stationary state. Simulations use a conventional pseudo-spectral method and second-order dissipation. Results were obtained on a 1024×1024 grid with long time averaging. Large-scale coherent vortices are clearly visible. Further details about the numerics and resulting velocity pdfs are described elsewhere [14, 15].

In many instances the velocity pdf is approximately Gaussian [16], and this is also the case for the simulated turbulence here [14]. Far more conclusive than the velocity distribution turns out to be the statistics of velocity derivatives. A number of authors have investigated the velocity gradients of three-dimensional Navier-Stokes turbulence [17, 18, 19, 20, 21, 22, 23, 24, 25], but here we consider the far less studied two-dimensional case. Measurements of the transverse velocity derivatives are presented in section II. Section III discusses evidence that large eddies alone provide only a minor contribution to the observed statistics. Section IV briefly discusses pertinent differences between forced and unforced turbulence. The last section contains conclusions.

II. THE PROBABILITY DISTRIBUTION OF VELOCITY DERIVATIVES

Earlier work based on satellite altimeter data reported transverse velocity gradient pdfs in small parts of the ocean [7]. These results differed from gradient pdfs derived for decaying two-dimensional turbulence, which showed an approximate Cauchy distribution during the late stage of the evolution [26, 27]. The discrepancy is resolved by comparing to simulations of stationary turbulence.

Figure 1 shows velocity gradient pdfs derived from ocean observations and simulations. The solid line indicates the pdf of normalized velocity gradient data derived from global satellite altimetry. To determine the oceanic pdf, velocity gradient data drawn from latitudes between 10° and 60°N and between 10° and 60°S are sorted geographically into 2.5° by 2.5° boxes. Data near the equator are omitted because the geostrophic relationship is weak at low latitudes. The standard deviation of gradients in each latitude-longitude box varies from $1.4 \times 10^{-5} \text{ s}^{-1}$ near 60° latitude up to $6.4 \times 10^{-5} \text{ s}^{-1}$ near 10° latitude, with a median value of $1.9 \times 10^{-5} \text{ s}^{-1}$. To compensate for this geographic variation, gradients are normalized to have unit standard deviation in each box, and then the pdf is computed from all of the normalized gradient data. For comparison, we also normalized our pdfs using the mean absolute value of the velocity gradient; this did not diminish the strong tails of the gradient pdf.

The dashed line in Fig. 1 represents the transverse velocity gradient pdf from two-dimensional Navier-Stokes turbulence. The dotted lines represent the narrow Gaussian distribution and the broader Cauchy distribution, $P(x) = c/[\pi(c^2 + x^2)]$, with long tails. The tails con-

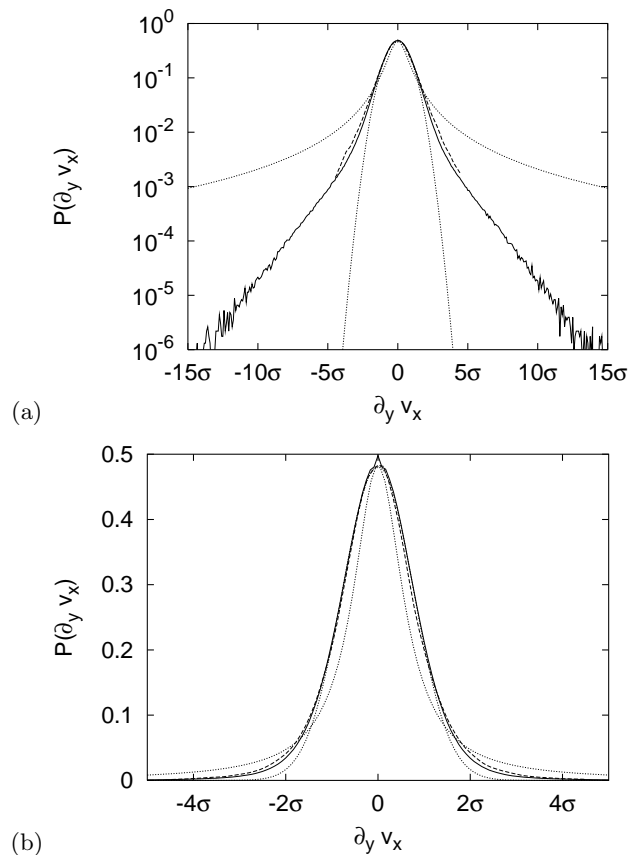


FIG. 1: (a) Global variance-normalized pdf of the velocity gradient in the ocean (solid line) compared with simulations of two-dimensional Navier-Stokes turbulence (dashed line) on a semi-logarithmic scale. (b) Same quantities on a linear scale. In both cases, a Gaussian and a Cauchy distribution are shown for comparison (dotted lines). The ocean pdf is averaged over about 13 million data points. Data are normalized by the standard deviation σ , as described in the text.

tribute noticeably to the standard deviation of the pdf, and therefore the Gaussian is fitted to the data without requiring unit area and unit standard deviation. This is necessary to make the Gaussian closely approximate the central part of the pdf. Since the Cauchy distribution cannot be normalized by its standard deviation, the constant c is chosen such that $P(0)$ matches. Both the simulated and observed gradient pdfs appear Gaussian for small velocity gradients, up to about one standard deviation. For large gradients they decay significantly more slowly than do Gaussian tails but substantially faster than the Cauchy distribution found in simulations of decaying turbulence [26, 27]. There is good agreement between observed and simulated pdfs up to even the largest fluctuations measured in the simulation.

Error bars for the pdfs were estimated by grouping the data into N groups and computing pdfs for each group. Error of the mean pdf is then taken to be the standard deviation of the pdf divided by \sqrt{N} . For this analysis, N

was the total number of 2.5° boxes for the surveyed ocean or the number of velocity snapshots for the simulation. Since many ocean observations are available, statistical errors are expected to be small compared to systematic errors. In fact, the statistical errors are frequently narrower than the line width in Fig. 1. Differences between the two distributions exceed the statistical errors and are likely to be due to a number of factors, including instrumental and atmospheric correction errors in the altimeter data, which make the measurements noisy, as well as differences in the physics of two-dimensional Navier–Stokes equations compared with the ocean.

The kurtosis (flatness), $\langle x^4 \rangle / \langle x^2 \rangle^2$, can serve as quantitative comparison of the shape of the pdf. In the simulation results, the velocity gradient pdf has a kurtosis of 4.7, indicating clear deviation from Gaussian distribution. If the observed ocean pdf is terminated beyond the extent of the simulated one, at about four and a half standard deviations, its kurtosis is also 4.7. This quantitative comparison confirms that the oceanic pdf is substantially better matched by the simulation than by either of the two ideal distributions.

Velocity gradient pdfs depend on the spatial separation between velocity measurements. The velocity correlations between two points decrease with distance, and velocities at points very far apart can be assumed to be statistically independent. The distribution of velocity differences across very large distances reduces to that of the velocity (with twice the variance). The 12 km separation of TOPEX observations is small compared with the decorrelation length scales of wind forcing, $O(1000 \text{ km})$, and of mesoscale ocean features $O(100 \text{ km})$, so velocities at adjacent observation points are expected to be strongly correlated. Therefore, to obtain comparable results from the numerical simulation, we have computed gradient pdfs from velocity differences over asymptotically small separations. For comparison, if we compute gradient pdfs over progressively larger distances in the simulation, then the distribution narrows from its original shape (dashed line in Fig. 1) and becomes close to Gaussian.

The basic simulations had a large-scale Reynolds number on the order of 10^4 , while for ocean turbulence a Reynolds number of 10^7 might be typical [28]. Pdfs were also determined for simulations with lower and higher Reynolds numbers, using respectively lower and higher resolutions, but shorter sampling time. There is no significant change in the shape of the pdfs [29], although these data do not exclude a weak dependence on Reynolds number. The absence of any detectable Reynolds number dependence suggests that the simulation data are close to what they look like at substantially higher Reynolds number. The difference in the length of the tails in Fig. 1 may be due to the vast difference in Reynolds number, difference in sampling size, and errors from the numerical differentiation of data.

The real ocean differs from the forced Navier–Stokes system because of the addition of the β -effect, stratifica-

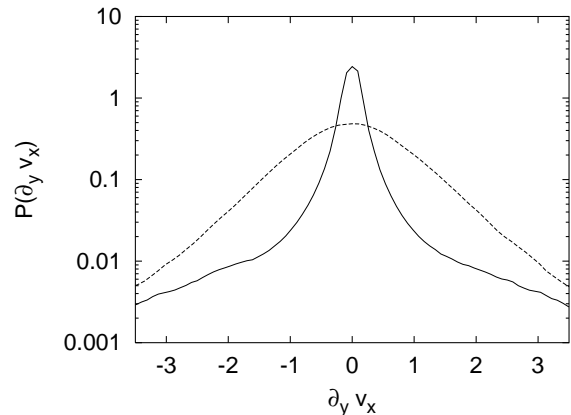


FIG. 2: Pdf of the velocity gradient in simulations of two-dimensional Navier–Stokes turbulence. The solid line is for the velocity gradients produced by large coherent vortices. The dashed line corresponds to the complete flow field. Both distributions are normalized by the same standard deviation, hence preserving differences in their width.

tion, three-dimensional motions, and buoyancy. Hence it is surprising that there is such a close agreement between measurement and simulation. In any case, the agreement between observation and simulation suggests that the oceanic velocity statistics may be understood within the framework of two-dimensional turbulence.

III. THE ROLE OF COHERENT VORTICES

Idealized models of point vortices predict a Cauchy distribution for the velocity gradients and a Gaussian distribution for the velocity [26, 27, 30, 31, 32]. This agrees with results from decaying two-dimensional turbulence [26, 33]. Hence, in the late stages of decay, the statistics of velocity gradients have been successfully understood to result from the far-field of well-separated vortices [26, 27]. In contrast, pdfs of ocean surface velocity gradients are observed to have more rapidly decaying tails than do Cauchy distributions. Also as Fig. 1 makes evident, the simulations of stationary two-dimensional turbulence show far less pronounced tails than a Cauchy distribution.

The discrepancy arises not only in the shape of the distribution but also in its width. A straight-forward way of illustrating this is to calculate the velocity field produced by vortices with vorticities that exceed twice the root-mean-square value. Figure 2 shows the transverse velocity gradients produced by these coherent vortices (solid line). For comparison, the actual distribution is shown as a dashed line. Clearly the large coherent vortices do not generate enough intermediate gradients. (Nor, for that matter, do they account for most of the vorticities.) Consequently, the distribution of gradients is poorly accounted for by large-scale coherent vortices.

The contribution of the small-scale turbulence is also

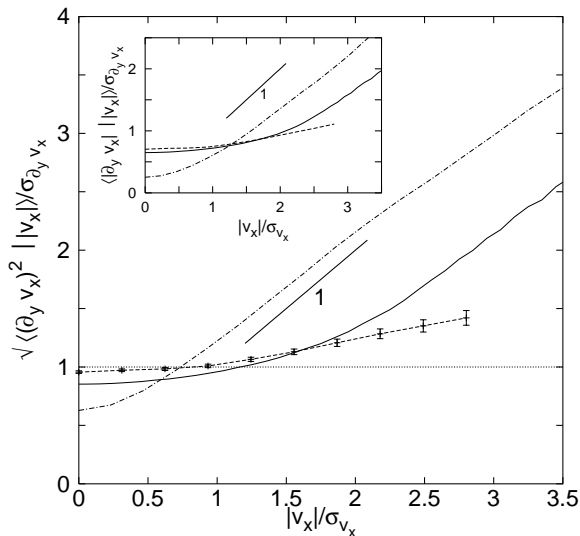


FIG. 3: Conditional average of transverse velocity gradient with velocity, $\sqrt{\langle (\partial_y v_x)^2 | |v_x| \rangle}$, for two-dimensional Navier-Stokes (dashed line with error bars) and ocean turbulence (solid line). The conditional average produced by the large vortices in the simulation is also shown (dash-dotted line). All three graphs are normalized by their respective standard deviations. The thick solid line indicates growth proportional to the velocity. The error bars include only the statistical error expected from averaging of the 32 snapshots, showing twice the standard error of the mean. The inset shows the conditional average of the absolute value $\langle |\partial_y v_x| | |v_x| \rangle$.

relevant. This agrees with the basic physical picture, according to which the late stage of decaying turbulence consists of coherent vortices. Its statistics can therefore be understood in terms of them. In the stationary case, on the other hand, fluctuations over a wide spectrum of spatial scales contribute to the gradient statistics.

Available statistical variables from the altimeter are the velocity and the transverse velocity derivative. Hence, one can study the cross-correlation between these two quantities. Here, we examine the conditional average of the squared velocity gradient as a function of velocity, $\langle (\partial_y v_x)^2 | |v_x| \rangle$, which is the average of $(\partial_y v_x)^2$ over all points with velocity component $\pm v_x$. The slope of $\langle (\partial_y v_x)^2 | |v_x| \rangle$ is a measure of the correlation between the velocity and the transverse velocity derivative. If there were no correlation between the velocity at a point and the gradient at the same point, the conditional average would be constant for all values of v_x and would be exactly one if velocity gradients were normalized by their standard deviation. In contrast, if gradients and velocities were strongly correlated, as would be expected around an isolated vortex, then the graph for the conditional average would have a pronounced slope.

Figure 3 shows the square-root of the measured conditional average together with that for two-dimensional Navier-Stokes turbulence. For the ocean, we have normalized both v_x and $\partial_y v_x$ by their standard deviations

in each 2.5° by 2.5° geographic box, because both quantities vary spatially. The axes are labeled in units of their respective standard deviations, $\sqrt{\langle v_x^2 \rangle}$ and $\sqrt{\langle (\partial_y v_x)^2 \rangle}$. The correlation between velocity and its gradient is weak, but the gradients tend to be higher when the velocity is large. If oceanic gradients beyond four standard deviations are excluded, which is a fairer comparison with the simulation, the conditional average is closer to one. The longitudinal component of the conditional average (not shown) exhibits behavior similar to the transverse component. Also shown in Fig. 3 is the conditional average for the velocity field of vortices larger than twice the root-mean-square vorticity (dash-dotted line). As expected there is a comparatively strong correlation between velocities and velocity derivatives. At large velocities the slopes of the graphs for the coherent vortices and the ocean are similar. This may indicate influence by large eddies in regions where the velocities are high, although no corresponding evidence is found in the probability distribution of the gradients. The situation at high velocities is therefore somewhat ambiguous. For small velocities, which cover most of the area, conditional averages are near one for simulations (dashed line) and observations (solid line), indicating that at low velocity, gradients are almost uncorrelated with velocity. The inset in Fig. 3 shows the conditional average using $|\partial_y v_x|$ instead of $(\partial_y v_x)^2$, which is less sensitive to outliers. For small velocities, the agreement between observation and simulation is closer and the discrepancy between the large eddy field and the other two conditional averages is stronger.

The deviation of the observed conditional averages from that for coherent vortices strengthens the evidence that the gradient statistics are unaccounted for by the velocity field created by large-scale coherent eddies. The role of coherent vortices in generating the observed velocity statistics is minor. This conclusion cautions against attempts to model oceanic velocity fields by large eddies.

IV. FORCED VERSUS UNFORCED TURBULENCE

Although only the transverse velocity component can be determined from altimeter data, simulations also permit us to examine the longitudinal derivative, $\partial_x v_x$. Figure 4 shows a clear difference between the behavior of the longitudinal and transverse components. In our forced simulations, the standard deviation of longitudinal fluctuations is about 60% of that for transverse fluctuations. In isotropic and incompressible turbulence there is an exact relation between the standard deviation of transverse and longitudinal component [34]. With a calculation analogous to the well-known three-dimensional case [34], we find in the two-dimensional case $\langle (\partial_y v_x)^2 \rangle = 3 \langle (\partial_x v_x)^2 \rangle$. Hence, the standard deviation for the longitudinal component is $1/\sqrt{3} \approx 58\%$ of that for the transverse component. This agrees with the measured value of 60% in the simulation.

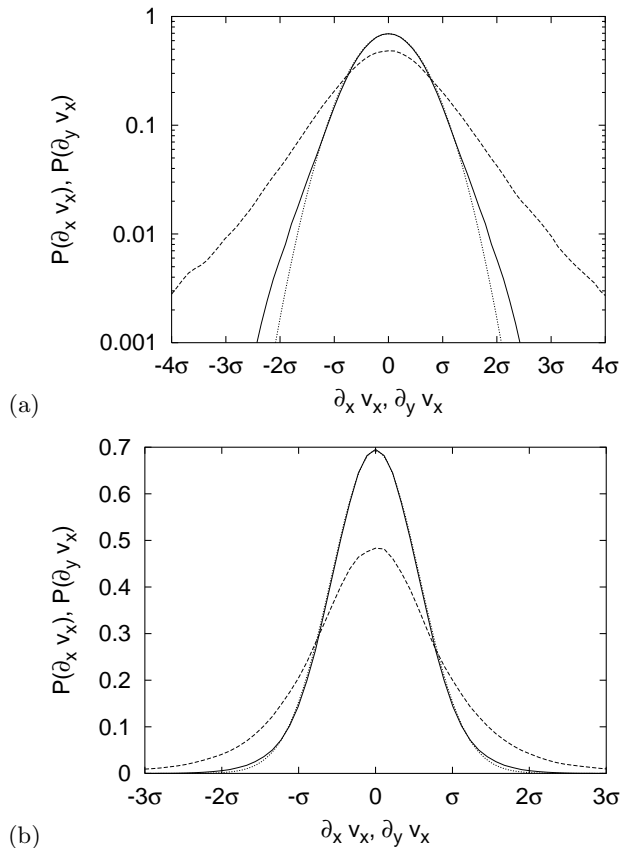


FIG. 4: (a) Probability density functions of velocity derivatives for forced two-dimensional Navier-Stokes turbulence on a semi-logarithmic scale. (b) Same quantities on a linear scale. In both panels, the dashed line shows the transverse component, $\partial_y v_x$, and the solid line the longitudinal component, $\partial_x v_x$. Both are normalized by the standard deviation of the transverse component $\sigma = \sqrt{\langle (\partial_y v_x)^2 \rangle}$. The dotted line is a Gaussian. Transverse and longitudinal gradient pdf differ from each other in width and shape.

Longitudinal and transverse pdfs differ not only by a factor of $\sqrt{3}$ in their standard deviation, but also in their shape. While the transverse gradients strongly deviate from a Gaussian distribution, the longitudinal gradient pdf more closely approximates a Gaussian. The kurtosis of the longitudinal component is 3.5, substantially closer to the Gaussian value of 3 than the transverse component is, implying that large longitudinal gradients occur less

frequently than do large transverse gradients. For simple point-vortex models both, transverse and longitudinal components, are distributed like Cauchy distributions (albeit with different standard deviations) [26]. Also in the late stage of decaying turbulence, the transverse component is distributed in the same way as the longitudinal component [26]. This is yet another difference between forced and unforced turbulence.

Overall, our study establishes a clear distinction between the gradient statistics of unforced (freely decaying) and forced (stationary) turbulence. The presence of forcing not only influences the properties of large-scale vortices but also changes the distribution of eddies over different scales. (Freely decaying turbulence has an inverse energy cascade while two-dimensional turbulence forced at large scales is governed by a direct enstrophy cascade.) Further study is needed to determine how the statistics may depend on the temporal and spatial structure of the forcing.

V. CONCLUSIONS

In conclusion, we find that transverse velocity derivative pdfs from observed upper-ocean turbulence agree closely with forced two-dimensional simulations but differ from previously reported unforced turbulence. The forcing diminishes the role of coherent vortices in the pertinent statistics. The distribution and cross-correlation of velocity derivatives provide clear evidence that large coherent eddies play only a minor role in generating the observed statistics. Further study of forced two-dimensional turbulence appears likely to shed light on the character of meso-scale turbulence in the ocean.

Acknowledgments

The work of N.S. was supported by a grant from the Research Grants Council of the Hong Kong Special Administrative Region, China (RGC Ref. No. CUHK4119/98P), by a postdoctoral fellowship from the Chinese University of Hong Kong, and by the Massachusetts Institute of Technology. S.T.G. was supported by NASA through the Jason Altimeter Science Working Team (JPL contract 1204910).

-
- [1] A. S. Monin and A. M. Yaglom, *Statistical Fluid Mechanics* (MIT Press, Cambridge, Massachusetts, 1975).
 - [2] C. Wunsch and D. Stammer, *Annu. Rev. Earth Planet. Sci.* **26**, 219 (1998).
 - [3] P. B. Rhines, *Annu. Rev. Fluid Mech.* **11**, 401 (1979).
 - [4] J. C. McWilliams, *J. Fluid Mech.* **146**, 21 (1984).
 - [5] M. M. Yale, D. T. Sandwell, and W. H. F. Smith, *J. Geophys. Res.* **100**, 15117 (1995).
 - [6] R. H. Stewart, C. K. Shum, B. Tapley, and L. Ji, *Physica D* **98**, 599 (1996).
 - [7] S. G. Llewellyn Smith and S. T. Gille, *Phys. Rev. Lett.* **81**, 5249 (1998).
 - [8] S. T. Gille and S. G. Llewellyn Smith, *J. Phys. Oceanogr.* **30**, 125 (2000).
 - [9] S. Houry, E. Dombrowsky, P. DeMey, and J.-F. Minster, *J. Phys. Oceanogr.* **17**, 1619 (1987).

- [10] D. Stammer, *J. Phys. Oceanogr.* **27**, 1743 (1997).
- [11] A. Bracco, J. H. LaCasce, and A. Provenzale, *J. Phys. Oceanogr.* **30**, 461 (2000).
- [12] W. G. Large, W. R. Holland, and J. C. Evans, *J. Phys. Oceanogr.* **21**, 998 (1991).
- [13] C. K. Wikle, R. F. Miliff, and W. G. Large, *J. Atmos. Sci.* **56**, 2222 (1999).
- [14] N. Schorghofer, *Phys. Rev. E* **61**, 6568 (2000).
- [15] N. Schorghofer, *Phys. Rev. E* **61**, 6572 (2000).
- [16] U. Frisch, *Turbulence* (Cambridge University Press, Cambridge, 1995).
- [17] S. Kida and Y. Murakami, *Fluid Dyn. Res.* **4**, 347 (1989).
- [18] R. H. Kraichnan, *Phys. Rev. Lett.* **65**, 575 (1990).
- [19] A. Vincent and M. Meneguzzi, *J. Fluid Mech.* **225**, 1 (1991).
- [20] K. Yamamoto and T. Kambe, *Fluid Dyn. Res.* **8**, 65 (1991).
- [21] U. Frisch and Z. S. She, *Fluid Dyn. Res.* **8**, 139 (1991).
- [22] R. Benzi, L. Biferale, G. Paladin, A. Vulpiani, and M. Vergassola, *Phys. Rev. Lett.* **67**, 2299 (1991).
- [23] S. Chen, G. D. Doolen, R. H. Kraichnan, and Z. S. She, *Phys. Fluids A* **5**, 458 (1993).
- [24] F. Belin, J. Maurer, P. Tabeling, and H. Willaime, *Phys. Fluids* **9**, 3843 (1997).
- [25] H. S. Shafi, Y. Zhu, and R. A. Antonia, *Fluid Dyn. Res.* **19**, 169 (1997).
- [26] J. Jimenez, *J. Fluid Mech.* **313**, 223 (1996).
- [27] I. A. Min, I. Mezic, and A. Leonard, *Phys. Fluids* **8**, 1169 (1996).
- [28] G. L. Mellor, *Introduction to Physical Oceanography* (Springer-Verlag, New York, 1996).
- [29] H. Takahashi and T. Gotoh, *Proc. Res. Inst. Math. Sci. (Kyoto Univ.)* **972**, 163 (1996).
- [30] B. N. Kuvshinov and T. J. Shep, *Phys. Rev. Lett.* **84**, 650 (2000).
- [31] P. H. Chavanis and C. Sire, *Phys. Rev. E* **62**, 490 (2000).
- [32] P. H. Chavanis and C. Sire, *Phys. Fluids* **13**, 1904 (2001).
- [33] P. Arroyo, G. Pedrizzetti, C. Vasco, and J. Jimenez, in *Advances in Turbulence V*, edited by R. Benzi (Kluwer, 1995), p. 11.
- [34] G. K. Batchelor, *The Theory of Homogeneous Turbulence* (Cambridge University Press, Cambridge, 1953).